Barrier hopping, viscous flow, and kinetic gelation in particle-polymer suspensions

Y.-L. Chen,* V. Kobelev, and K. S. Schweizer†
Department of Materials Science & Engineering and Frederick Seitz Materials Research Laboratory, University of Illinois, 1304 West Green Street, Urbana, Illinois 61801, USA
(Received 22 October 2004; published 27 April 2005)

The naive mode coupling–polymer reference interaction site model (MCT-PRISM) theory of gelation and elasticity of suspensions of hard sphere colloids or nanoparticles mixed with nonadsorbing polymers has been extended to treat the emergence of barriers, activated transport, and viscous flow. The barrier makes the dominant contribution to the single particle relaxation time and shear viscosity, and is a rich function of the depletion attraction strength via the polymer concentration, polymer-particle size asymmetry ratio, and particle volume fraction. The dependences of the barrier on these three system parameters can be accurately collapsed onto a single scaling variable, and the resultant master curve is well described by a power law. Nearly universal master curves are also constructed for the hopping or α relaxation time for system conditions not too close to the ideal MCT transition. Based on the calculated barrier hopping time, a theory for kinetic gel boundaries is proposed. The form and dependence on system parameters of the kinetic gel lines are qualitatively the same as obtained from prior ideal MCT-PRISM studies. The possible relevance of our results to the phenomenon of gravity-driven gel collapse is studied. The general approach can be extended to treat nonlinear viscoelasticity and rheology of polymer-colloid suspensions and gels.

DOI: 10.1103/PhysRevE.71.041405 PACS number(s): 82.70.Dd, 83.60.Bc, 83.10.−y

I. INTRODUCTION

Physical gels, formed via attractive intermolecular interactions, are viscoelastic amorphous materials that behave as either solids or liquids depending on the time scale. For model suspensions of nonadsorbing polymers and hard sphere colloids, the origin of the interparticle attraction is the entropic "depletion effect" [1,2] which can be exquisitely tuned by varying the polymer and particle sizes, polymer concentration, particle volume fraction, and solvent quality. The equilibrium and nonequilibrium phase behavior, fluid structure, and thermodynamic properties of such suspensions have been extensively studied recently [3–20]. Experiments find that with increasing polymer concentration (depletion attraction) a fluid-fluid phase separation is first observed if the polymer radius of gyration (R_g) to particle radius (R) "size asymmetry ratio" R_g/R is greater than roughly 0.3 [8]. In the $0.1<R_g/R<0.3$ regime, an equilibrium fluid-crystal transition occurs for nearly monodisperse particles. If $R_g<0.1R$, the dilute polymer additives generally induce a direct one-phase fluid-gel nonequilibrium transition [8–10,12,15].

Depending on polymer concentration (c_p), particle volume fraction ($\phi=\pi\rho_s D^3/6, D=2R$), and size asymmetry ratio, the gel may maintain its solidlike mechanical properties for an indefinitely long time, or collapse and flow corresponding to "transient gelation" [8,16,20]. At relatively low volume fractions ($\phi<\phi_c\sim 0.2-0.3$) and/or close to the fluid-gel boundary (weak depletion attractions), "gels" can form as ergodic amorphous cluster deposits via kinetic aggregation and sedimentation [8,9,12], a process that generally occurs in the absence of buoyancy matching. At higher polymer concentrations and/or particle volume fractions ($\phi>\phi_c$), a nonergodic space-spanning network exists, which may or may not collapse and densify on the experimental time scale.

Much theoretical progress has recently been made [21–28] toward a microscopic understanding of the ergodic-nonergodic transition in sticky particle suspensions using the idealized mode coupling theory (IMCT) [29]. Recent combined theory-experiment studies [10,12,13,18,30] have been performed by Zukoski and co-workers for polymer-nanoparticle depletion systems where $R_g/R<0.1$. The gel microstructure, viscoelasticity, and gelation boundary have been measured and compared to a hybrid theoretical approach [26] which combines the simplest "naive" version of MCT [31] with accurate structure factor input from the two-component polymer reference interaction site model (PRISM) theory [5]. MCT-PRISM theory predicts effective power law dependences of the fluid-gel boundary and elastic modulus on R_g/R, c_p, and ϕ, which are in very good agreement with experiment [18,26]. The *qualitative* importance of many body effects beyond a dilute two-particle potential of mean force description (e.g., Asakura and Oosawa [1,2]) has been demonstrated [26,31].

A limitation of ideal MCT is that it is primarily a theory for the onset of strong caging and dynamical arrest. It does not include long time ergodicity restoring processes associated with barrier hopping. For glassy fluids the ideal MCT transition is often interpreted as signaling the transition to a new activated dynamical regime [29,32]. Recent computer simulations of dense sticky particle suspensions suggest the gel state predicted by MCT has a finite lifetime due to activated hopping events which break the attractive "bond" between colloids [33]. Long time hopping processes are likely

*Present address: Department of Chemical and Biological Engineering, University of Wisconsin–Madison, Madison, Wisconsin.
†Corresponding author. Electronic address: kschweiz@uiuc.edu

a crucial elementary event for phenomena such as physical aging, sedimentation, gel collapse, and transport in the extremely viscous regime. Recent experiments on polymer-colloid mixtures have studied the dependence of the gravity-driven depletion gel collapse time on system variables [34]. Measurements of the shear viscosity of depletion suspensions find systematic dependences on polymer concentration and volume fraction [35].

The goal of this paper is to extend the approach of Saltzman and Schweizer [32] for treating activated barrier hopping processes in colloidal glasses to the gelation problem. In Sec. II the naive MCT-PRISM and activated hopping theories are briefly reviewed. Numerical results for a "non-equilibrium free energy" are given and analyzed in Sec. III. Section IV presents calculations of the barrier hopping time and kinetic gel boundaries and application to the problem of gel collapse. The shear viscosity is studied in Sec. V. The paper concludes in Sec. VI with a brief discussion and summary.

II. THEORY

The two-component polymer–hard sphere particle model and PRISM theory [4,5], naive ideal MCT [26,31], and the barrier hopping approach [32] have all been discussed in great depth in prior publications. There are three key system parameters: the polymer-particle size asymmetry ratio R_g/R, the polymer concentration c_p or its dimensionless version c_p/c_p^* where c_p^*, is the dilute-semidilute crossover concentration [36], and the particle volume fraction ϕ. We consider the athermal or good solvent entropy controlled regime, which corresponds to monomer-monomer excluded volume interactions between the threadlike chains and between monomers and particles [5]. An version of PRISM theory [5] that self-consistently includes the consequences of nonlocal conformational entropy effects is employed to determine the three pair correlation functions and partial static structure factors which are the required input to naive MCT and its activated barrier hopping generalization.

Our focus is not on the ultrahigh particle volume fraction regime where glassy physics is dominant and/or strongly interferes with attraction-driven gelation [28]. The very low volume fraction regime is also not of prime interest. Rather, our main focus is the moderately concentrated ($\phi \sim 0.1-0.4$) and highly size asymmetric ($R_g/R \ll 1$) regime where direct nonergodic fluid-gel transitions often occur.

A. Naive MCT-PRISM theory

Naive MCT [31] combined with two-component PRISM theory [5] allows predictions of the ergodic-nonergodic gel boundary, particle localization length, and elastic shear modulus. A standard dynamically effective one-component approach is adopted [20–27,37]. The key quantity is the long time limit of the force-force time correlation function experienced by a single particle, $K(t\to\infty)=\langle \vec{f}(0)\cdot\vec{f}(t\to\infty)\rangle$. The long time limit of the particle displacement plays the role of a scalar dynamic order parameter, $r_{\rm loc} = \sqrt{\langle [r(t\to\infty)-r(t=0)]^2\rangle}$, which obeys the self-consistent equation [32]

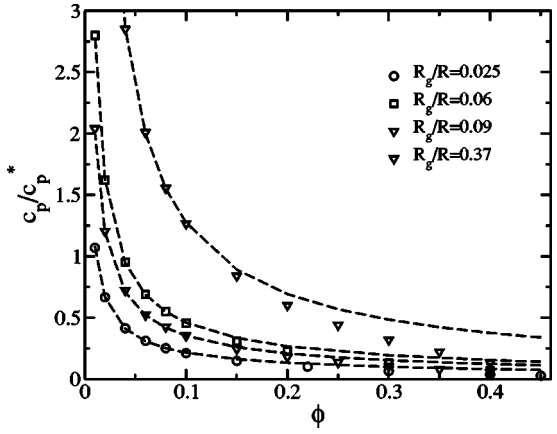

FIG. 1. Naive MCT-PRISM theory predictions of the ideal gel transition boundaries for $R_g/R=0.025$, 0.06, 0.09, and 0.37. Dashed lines are power law curve fits for the lower ϕ region.

$$\alpha = \frac{1}{12\pi^2}\int_0^\infty dq[q^4\rho_s\hat{C}^2(q)\hat{S}(q)e^{(q^2/4\alpha)[1+1/S(q)]}] \qquad (1)$$

where q is the wave vector, $\alpha=3/(2\ r_{\rm loc}{}^2)$, ρ_s is the particle number density, and $\hat{C}(q)$ and $\hat{S}(q)$ are the *effective* direct correlation function [26,37] and dimensionless colloid collective structure factor calculated from *two-component* PRISM theory, respectively. Equation (1) determines the polymer and particle densities that define a gel boundary as when one nonzero α (localized) solution emerges. Representative results are shown in Fig. 1. Prior work has established that the shape of the gel boundary is a fractional power law at relatively low ϕ and exponential at high volume fractions, and the gel boundaries shift up with increasing size asymmetry ratio [26]. For relatively low volume fractions one finds

$$\frac{c_p^{\rm gel}}{c_p^*} = A\phi^{-y}, \quad \phi \leqslant 0.2-0.3, \qquad (2)$$

where $y\sim 0.7-0.9$ and is a weakly increasing function of R_g/R, and $A\propto\sqrt{R_g/R}$ and varies from $\sim$0.04 to 0.17 over the wide range of size asymmetry $R_g/R=0.025-0.37$. At higher volume fractions the gel boundary has an exponential form:

$$-\ln(\phi) = a + bU, \quad \phi \geqslant 0.2-0.3,$$

$$U \equiv \frac{3}{2}\frac{c_p^{\rm gel}}{c_p^*}\frac{R}{R_g} \qquad (3)$$

where $a\sim 1$, and b increases from $\sim$0.15 to 0.34 as the size asymmetry ratio R_g/R increases from 0.025 to 0.37 [26]. The quantity U is the strength at contact of the classic Asakura-Oosawa (AO) depletion attraction [1,2]. The predicted shapes and trends of the gel boundaries are in good agreement [26] with several experiments [9,12,16,20] under conditions where sedimentation of cluster aggregates does not occur. Calculations of the elastic modulus are also in accord

with experiment where novel effective power law scalings with R_g/R, c_p, and ϕ are predicted and observed [18,26,30]. The importance of polymer-induced particle structural reorganizations on the R_g scale in determining the predictions of MCT-PRISM theory has been explicitly documented [26,30].

B. Barriers and hopping transport

To treat activated processes the IMCT nonergodicity transition is interpreted as signaling the emergence of finite barriers in a dynamically defined landscape and strong *transient* localization. As discussed in depth previously [32], the beyond MCT approach has not been rigorously derived, but can be motivated in two distinct, *but equivalent in practice*, ways. Briefly, the first motivation is in the spirit of Brownian motion or Kramers theory. The central dynamical quantity is the scalar single particle dynamical variable $r(t)$, the *displacement* of a particle from a random initial location. The second motivation is in the spirit of dynamic density functional theory [38], or time-dependent Landau-Ginzburg theory for a nonconserved order parameter [39], where $r(t)$ is a particle displacement partially averaged (coarse grained) over space and time. The theory is based on a stochastic equation of motion for $r(t)$ the construction of which is guided by three ideas. (1) The short time motion is Fickian diffusion. (2) In the absence of thermal fluctuations (noise), ideal MCT ' is assumed to correctly predict the tendency to localize in a cage. Hence, in the deterministic limit the naive IMCT localization condition should be recovered. This idea guides the construction of a *displacement-dependent* effective caging *force* $-\partial F/\partial r$, which favors localization. F is called a "nonequilibrium" or "effective" free energy but does *not* have a rigorous equilibrium meaning. (3) Ergodicity restoring fluctuations destroy the naive MCT glass transition via activated hopping.

The resulting nonlinear stochastic equation of motion for $r(t)$ in the overdamped limit corresponds to a force balance [32]:

$$-\zeta_s \frac{d}{dt} r - \frac{\partial}{\partial r} F + \delta f = M \frac{d^2}{dt^2} r = 0 \tag{4}$$

where ζ_s is a short time friction constant due to binary collisions [40], $\zeta_s = \zeta_0 g(D)$, $\zeta_0 = k_B T / D_0 = 3\pi D \eta_0$ is the Stokes-Einstein friction constant, η_0 is the solvent viscosity, D_0 is the Stokes-Einstein diffusion constant, and $g(D)$ is the contact value of the particle radial distribution function [41]. The use of two-particle hydrodynamics to quantify the short time friction constant yields nearly identical results for hard sphere colloids [32]. The white noise fluctuating force is taken to be statistically uncorrelated with the tagged particle position and velocity and satisfies $\langle \delta f(0) \delta f(t) \rangle = 2\beta^{-1} \zeta_s \delta(t)$. This choice is made in analogy with the stochastic description of the scalar dynamic variable (reaction coordinate) in Kramers theory or a nonconserved scalar order parameter of model A of dynamic critical phenomena [39]. In principle the noise can be multiplicative which would be a serious technical complication. A derivation of the present approach based on the single particle density field as the central quantity has recently been achieved and the noise is multiplicative [42].

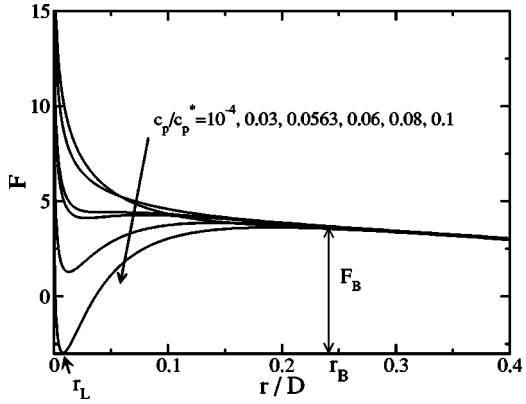

FIG. 2. The "nonequilibrium" free energy per particle (in units of k_BT) for $R_g/R = 0.06$, $\phi = 0.4$. The ergodic-nonergodic transition is found at $c_p/c_p^* = 0.0563$, where a local minimum first emerges. The localization length (r_L), barrier location (r_B), and barrier height (F_B) are indicated.

Although description of the derivation is beyond the scope of the present paper, it has been shown that Eq. (4) follows from a contraction and closure of the equation of motion for the density field at the simplest level of the scalar mean square displacement. At this level the fluctuating forces are described by the simple white noise form originally adopted in heuristically motivated theory.

A nonequilibrium "free energy" per particle (in units of k_BT) is introduced to quantify the *difference* between localized (nonzero α) and delocalized ($\alpha = 0$) states. It is constructed in the spirit of density functional theory [31,32,38]:

$$F(\alpha) = \frac{3}{2} \ln \alpha - \frac{1}{2\pi^2} \int dq\, \rho_s q^2 C(q)^2 \frac{S(q)^2}{1 + S(q)} \times \exp\left[\frac{-q^2}{4\alpha} \left(1 + \frac{1}{S(q)} \right) \right]. \tag{5}$$

The leading "ideal" term favors the fluid state, and is of a strongly localized form which is adequate for our purpose of describing the local barrier hopping processes on the less than one particle diameter length scale [32]. The second "interaction" contribution corresponds to an entropic trapping potential favoring localization. Minimization of Eq. (5) with respect to α, or solution of Eqs. (4) and (5) in the absence of noise, yields the naive MCT localization condition of Eq. (1). Beyond the ideal MCT gel boundary an intensive barrier F_B and local minimum and maximum appear in $F(r)$. An example is shown in Fig. 2 where c_p/c_p^* is the control parameter. Characteristic lengths include the location of the minimum ("localization length" r_L), local maximum (barrier location r_B), and a "diffusion length" L_D, defined as the displacement beyond which the interaction part of the caging force is negligible [32]. As polymer concentration increases beyond the ideal MCT transition value c_p^{gel}, the location and height of the barrier increase and the localization length decreases.

The mean first passage, or hopping, time follows from Kramers' theory [43] in the high friction, overdamped (diffusive barrier crossing) limit as [32]

$$\frac{\tau}{\tau_0} = \frac{2\pi g(D)}{\sqrt{K_0 K_B}} e^{F_B} \tag{6}$$

where $\tau_0 = D^2\zeta_0/k_BT$ is the elementary Brownian diffusion time, $g(D)$ is the colloid-colloid radial distribution function at contact, and K_0 and K_B are the absolute magnitudes of the well and barrier harmonic curvatures in units of k_BT/D^2, respectively. For a $D=100$ nm particle in toluene at room temperature $\tau_0 \sim 10^{-3}$ s. The use of $g(D)$ in the short time friction is well established in hard sphere suspensions where it quantifies the binary collision rate [40]. The situation for sticky colloids is far less understood due to the potential importance of both attractive and repulsive forces. Here we adopt the Enskog picture that the repulsive forces (binary hard core collisions) make the dominant contribution to the short time friction with depletion attractions only enhancing the collision rate. We have performed calculations based on two extreme choices for the contact value: the hard sphere Percus-Yevick result $g_{\rm HS}(D)$, and the full polymer-induced depletion attraction result $g(D)$, determined from two-component PRISM theory. Since the hopping time is dominated by the activated barrier contribution under the conditions of interest, this prefactor uncertainty introduces very little ambiguity in our theoretical analysis; unless stated otherwise all calculations employ $g(D)$. In the highly viscous fluid phase, the hopping time is expected to be closely correlated with the flow or structural relaxation time. Deep in the gel state it reflects the typical lifetime of a "depletion bond."

To compute macroscopic viscoelastic properties the Green-Kubo relations simplified by the standard MCT decoupling approximations are employed. The elastic shear modulus is calculated as in ideal MCT theory [20–29]:

$$G' \cong \frac{k_BT}{60\pi^2}\int_0^\infty dq\left(q^2\frac{\partial}{\partial q}\ln S(q)\right)^2 e^{-q^2/2S(q)\alpha}, \tag{7}$$

where the localization parameter α is computed from Eq. (1). In the highly viscous regime the shear viscosity can be estimated from a simple Maxwell model [44] argument as

$$\eta = \eta_\infty + G'\tau, \tag{8}$$

where $\eta_\infty = \eta_0 g(D)$ is the high frequency viscosity in the binary collision based approach [40]. Similarly, a hopping diffusion constant follows from Fick's law as

$$D_{\rm hop} \cong L_D^2/6\tau, \tag{9}$$

where L_D is simply estimated as $0.8D$ following prior work [32]. A full Green-Kubo calculation of the viscosity and self-diffusion constant also follows prior work [32]. The hopping contribution to the friction is combined with the accurate description of Cohen *et al.* for the short time "binary collisions in a mean field cage" aspect [40]. The shear viscosity is then given by [32]

$$\eta = \eta_\infty + \frac{k_BT}{120\pi^2}\int_0^\infty dq\, q^2\left(\frac{\partial}{\partial q}\ln S(q)\right)^2 \frac{1}{D_s^c(q)}. \tag{10}$$

The cage diffusion constant is

$$D_c^s(q) = \frac{D_0}{S(q)[g(D)d(q)^{-1} + (\zeta_{\rm hop}/\zeta_0)]} \tag{11}$$

where $d(q) = [1 - j_0(qD) + 2j_2(qD)]^{-1}$, $j_k(x)$ is the spherical Bessel function of order k, and the friction constant is a sum of the short time and hopping contributions,

$$\zeta_{\rm hop} = k_BT/D_{\rm hop} = 6k_BT\tau_{\rm hop}/L_D^2. \tag{12}$$

No adjustable parameter calculations of the relaxation time, shear viscosity, self-diffusion constant, and other quantities have been previously shown to be in good agreement with experiments on glassy hard sphere suspensions up to $\phi \sim 0.57-0.58$ [32].

III. NONEQUILIBRIUM FREE ENERGY

In this section numerical results are presented for the characteristic length and energy scales of $F(r)$. Emphasis is placed on identifying the dimensionless variable(s) that result in a master curve for the barrier and dynamic prefactor in Eq. (6).

A. Length scales

The location of the minimum of $F(r)$, or the localization length of MCT, r_L, is shown in Fig. 3(a) as a function of polymer concentration normalized by the MCT gel value for several different volume fractions and size asymmetry ratios. Nondimensionalization of r_L by the polymer radius of gyration (characteristic range of depletion attraction), and polymer concentration by its ideal MCT gel transition value, results in a rather good collapse for fixed volume fraction. As previously discussed [26], the localization length decreases as a power law with reduced polymer concentration,

$$r_L \propto (c_p/c_p^{\rm gel})^{-v} \tag{13}$$

with $v \sim 2-3$ for $c_p/c_p^{\rm gel} > 1.05$. This behavior is the origin of the MCT-PRISM theory prediction of a power law concentration dependence for the elastic shear modulus [18,26,30].

Figure 3(b) shows that the dependence of the barrier location r_B on system parameters is very different from that found for the localization length. With increasing polymer concentration or volume fraction the barrier location *increases*, and hence the "jump distance" from the minimum to the barrier maximum ("transition state") increases as the gel state is more deeply entered. In contrast to the localization length, nondimensionalization of the barrier location by R_g does not result in a near collapse of the results. Nondimensionalization by the particle diameter (not shown) yields a plot that is qualitatively the same as Fig. 3(b).

Physically, the barrier location can be interpreted as the displacement which most severely distorts the local structure. For sticky colloids, this distance is influenced by both the short range depletion attraction and the hard core repulsive forces. The relevance of two length scales qualitatively rationalizes the numerical calculations which find the magnitude of the barrier location is considerably larger than R_g but smaller than a particle radius. For example, for $c_p/c_p^{\rm gel} \sim 2$ and $\phi = 0.4$, the barrier location in units of the colloid

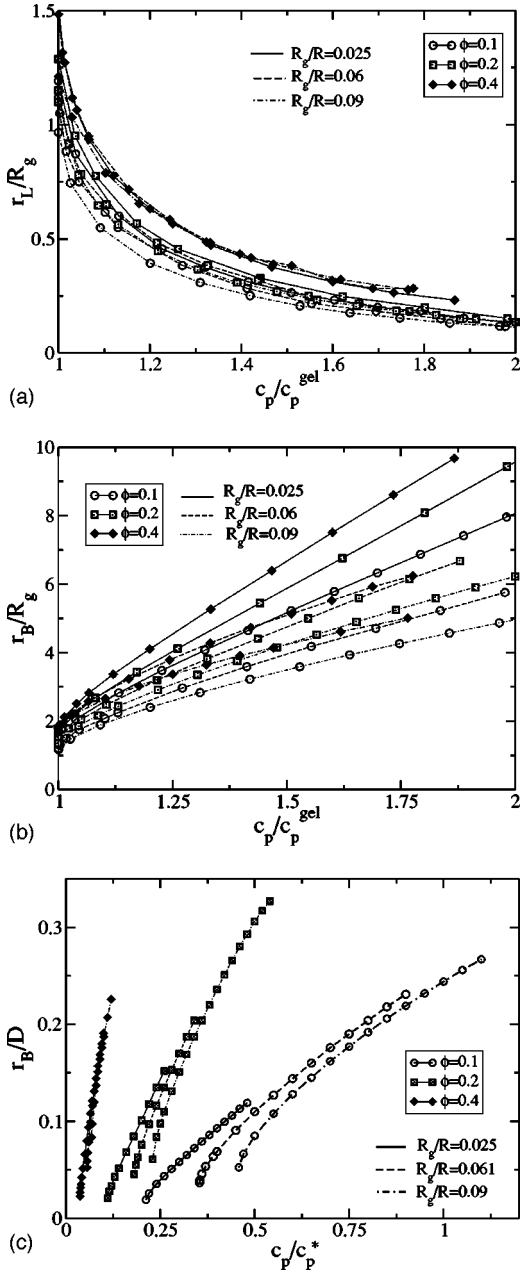

FIG. 3. (a) Reduced particle localization length as a function of c_p/c_p^{gel} for $R_g/R=0.025$ (solid lines), 0.06 (dashed lines), and 0.09 (dot-dashed lines) and volume fractions of $\phi=0.1$ (circles), 0.2 (squares), and 0.4 (diamonds). (b) Barrier location in units of the polymer radius of gyration as a function of c_p/c_p^{gel} for the same conditions as in (a). (c) Barrier location in units of the hard sphere diameter as a function of c_p/c_p^* for the same conditions as in (a).

diameter (R_g) is approximately 0.14 (11), 0.2 (6), and 0.25 (5) for $R_g/R=0.025$, 0.06, and 0.09, respectively. In contrast, for glassy hard sphere fluids [32] the barrier location varies from ~0.25 to 0.4 particle diameters as the volume fraction increases from 0.52 to 0.62. This suggests that the most unfavorable displacement in depletion gels is determined as a compromise between breaking the depletion attraction "bond" and disturbing the repulsive force aspects of cage structure. Evidence is presented in Fig. 3(c) that the latter

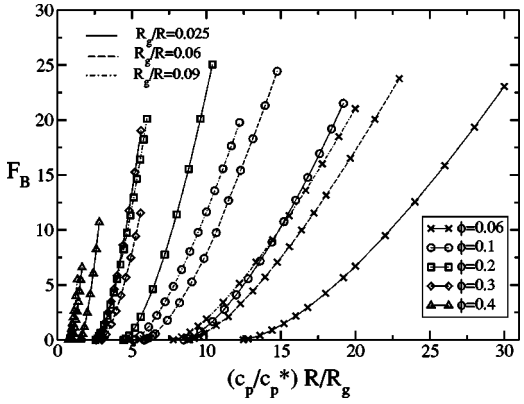

FIG. 4. Barrier height (in units of k_BT) for $R_g/R=0.025$ (solid lines), 0.06 (dashed lines), and 0.09 (dot-dashed lines) and $\phi=0.06$ (crosses), 0.1 (circles), 0.2 (squares), 0.3 (diamonds), and 0.4 (triangles) as a function of (c_p/c_p^*) (R/R_g).

aspect is most important deep in the gel (high c_p/c_p^{gel}) where the barrier location becomes nearly independent of the size asymmetry ratio (range of depletion attraction).

B. Barrier height

Figure 4 shows the barrier as a function of reduced polymer concentration multiplied by the inverse size asymmetry ratio; the abscissa has the same polymer concentration and size asymmetry dependence as the classic AO model [1,2] for the contact depletion attraction strength. Results for a wide range of colloid volume fractions and three size asymmetry ratios are given. At fixed c_p/c_p^* the barriers get larger with increasing (decreasing) ϕ (R_g/R). This trend simply reflects the ease of gelation at the ideal MCT level (Fig. 1). Qualitatively the same dependencies of F_B on c_p/c_p^* are obtained for different ϕ or R_g/R suggesting an underlying simplicity exists.

Our search for a scaling variable that can collapse the results in Fig. 4 is motivated by the relevance of polymer concentration compared to its critical MCT value $(c_p - c_p^{\mathrm{gel}})/c_p^*$. Figure 5 shows that the composite variable x defined as

$$x = A(\phi)(R_g/R)^{-3/4}(c_p - c_p^{\mathrm{gel}})/c_p^* \tag{14}$$

results in an excellent collapse of all the barrier height calculations. The shift factor in Eq. (14) is well described by a quadratic function

$$A(\phi) \sim 13.5\phi + 15.6\phi^2, \tag{15}$$

with deviations of less than 10%. Moreover, the master curve can be represented as a simple power law:

$$F_B = 1.35x^{1.46}. \tag{16}$$

This two-parameter representation is not unique; a parabolic fit (not shown) works nearly as well:

$$F_B = 1.3x + 0.29x^2. \tag{17}$$

Equations (14) and (16) imply a roughly linear dependence of the barrier on inverse size asymmetry ratio, $F_B \propto R/R_g$.

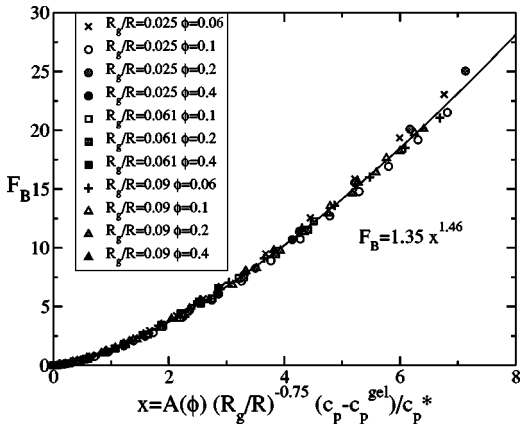

FIG. 5. Master plot of the barrier height as a function of the reduced variable $x=\mathrm{A}(\phi)\ (R/R_g)^{0.75}\ (c_p-c_p^{\mathrm{gel}})/c_p^*$ for $R_g/R=0.025$, 0.06, 0.09 over the volume fraction range $\phi=0.06-0.4$. The solid line is the two-parameter curve fit $F_B=1.35x^{1.46}$.

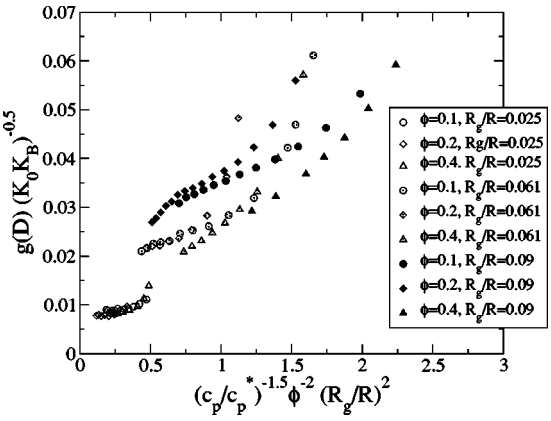

FIG. 6. Dynamical prefactor as a function of a composite variable for the several indicated values of volume fraction and size asymmetry ratio, and a range of reduced polymer concentrations. A rough linear correlation is found.

This trend is analogous to the simple Asakura-Oosawa model result for the contact depletion attraction of two large colloids dissolved at infinite dilution in an ideal (dilute) polymer solution [1,2]

$$W_{\mathrm{AO}}=\frac{3}{2}\frac{c_p}{c_p^*}\frac{R}{R_g}. \tag{18}$$

However, the nonlinear dependence of the barrier on polymer concentration, and strong dependence on colloid volume fraction, have no counterpart in the AO model. Physically, an increasing barrier with volume fraction makes sense in terms of the number of "bonded" neighbors or a sticky coordination number (number of neighbors within the depletion attraction range R_g) which PRISM calculations (not shown) find increases monotonically with ϕ in a manner qualitatively described by Eq. (15).

C. Dynamical prefactor

The well (K_0) and barrier (K_B) curvatures enter in the prefactor of the hopping time in Eq. (6) and depend on all the system variables. Multiple calculations (not shown) find that $K_0\sim 1/r_{\mathrm{loc}}^2$ (as previously found for hard sphere suspensions [32]), which implies the well curvature *grows* strongly with polymer concentration as a power law with exponents $\sim 4-6$. The barrier curvature *decreases* in a power-law-like fashion as $(c_p/c_p^{\mathrm{gel}})^n$, but more weakly since $n\sim -2$ to -3. The dynamical prefactor also involves the contact value of the particle radial distribution function, which increases rather gently with polymer concentration, particle volume fraction, and size asymmetry due to enhancement of the depletion-driven local particle clustering process [5].

To facilitate a compact representation of our numerical results in a form most appropriate for comparison with experiment, we have searched for empirical representations of our many calculations of the prefactor. For several size asymmetry ratios, volume fractions, and polymer concentrations not too close to the ideal MCT boundary, Fig. 6 shows that the dynamical prefactor roughly follows the scaling

$$\frac{g(D)}{\sqrt{K_0K_B}}\propto\left(\frac{c_p}{c_p^*}\right)^{-3/2}\phi^{-2}\left(\frac{R_g}{R}\right)^2. \tag{19a}$$

Clearly the dependence of the prefactor on system variables is far weaker than the exponential behavior of the barrier contribution to the hopping time. We do not claim the scaling in Eq. (19a) is unique, but the level of collapse it affords is meaningful since the barrier ranges from ~ 1 to 25 over the range of system parameters that define the abscissa in Fig. 6.

We have also empirically discovered (plots not shown) an alternative representation of the dynamical prefactor in terms of the polymer concentration reduced by its value at the ideal MCT gel transition and the composite variable x in Eq. (14). This representation is primarily of theoretical interest, and is given by

$$\frac{1}{\sqrt{K_0K_B}}=\left(\frac{R_g}{R}\right)^2(1.8+20x)^{-1},$$

$$g(D)=a_1+a_2x,$$

$$a_1\equiv 2(R_g/R)^{2/5}\phi^{-3/5},$$

$$a_2\equiv (R_g/R)(3.4+4\phi+20\phi^2). \tag{19b}$$

IV. LONG TIME DYNAMICS

By combining Eqs. (6), (14)–(16), and (19b), an approximate but rather accurate "universal expression" for the hopping time can be written down. However, such a collapse onto a master curve requires knowledge of the difference between the polymer concentration and its ideal MCT gel boundary value. The latter generally cannot be unambiguously extracted from experimental data. Hence, in this section we first present model calculations of the hopping time in a format relevant to experiment.

A. Activated hopping time

Numerical results are given in Fig. 7 for the dimensionless hopping time τ/τ_0 as a function of c_p/c_p^*, over a wide

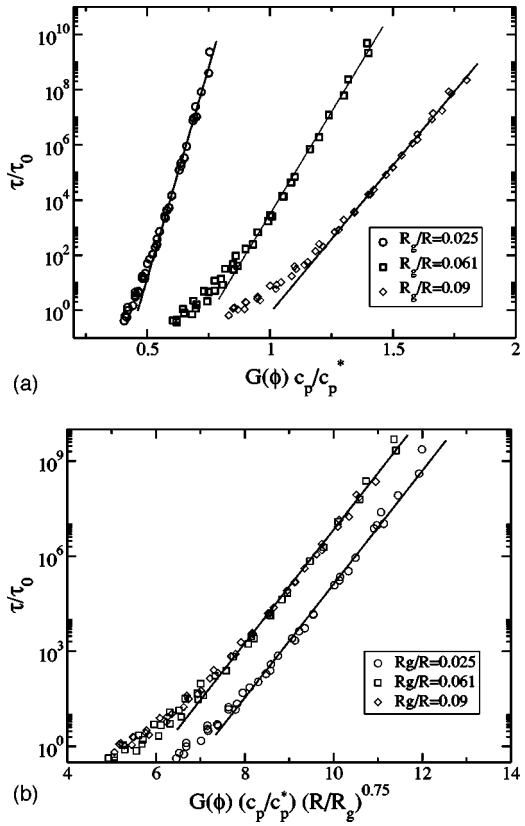

FIG. 7. (a) Activated hopping time (in units of the elementary Brownian time) as a function of $G(\phi)\ c_p/c_p^*$ for $R_g/R=0.025$ (circles), 0.061 (squares), and 0.09 (diamonds) over the range $\phi=0.06-0.4$. $G(\phi)$ is defined by Eq. (20). Solid lines are exponential fits. (b) Same data as in (a) but plotted as a function of $G(\phi)(c_p/c_p^*)(R_g/R)^{0.75}$. Solid lines are exponential fits.

range of volume fractions ($\phi=0.06-0.4$) and three size asymmetry ratios. Figure 7(a) constructs a master curve for the polymer concentration and particle volume fraction dependences at a *fixed* size asymmetry ratio. The concentration has been rescaled by a volume fraction (but R_g/R *independent*) function which empirically collapses all the volume fraction results,

$$G(\phi) = 0.5 + 7.8\phi + 27\phi^2. \tag{20}$$

This shift function differs from its counterpart $A(\phi)$ for F_B in Eq. (15) due to the contributions from the dynamical prefactor in Eq. (6). Beyond the low barrier regime (roughly $\tau/\tau_0 > 10-50$), the hopping time is an exponential function of reduced polymer concentration, and nearly an exponential function of volume fraction. The corresponding slope of the log-linear plots systematically increase with decreasing R_g/R.

Figure 7(b) shows that the slope variations of the hopping time in Fig. 7(a) can be collapsed over eight or more orders of magnitude variation by rescaling the control variable by the inverse size asymmetry ratio raised to the $\sim 3/4$ power. This results in curves of nearly identical shape given by

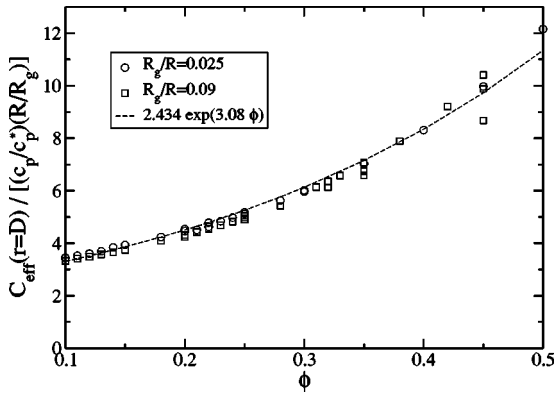

FIG. 8. The contact value of the effective interparticle direct correlation function scaled by $(c_p/c_p^*)(R/R_g)$ as a function of volume fraction for $R_g/R=0.025$ (circles) and 0.09 (squares). The dashed line is an exponential fit.

$$\ln(\tau/\tau_0) = Q + c_1 G(\phi)\frac{c_p}{c_p^*}\left(\frac{R}{R_g}\right)^{3/4} \equiv Q + F_{\text{eff}} \tag{21}$$

where $c_1 \sim 4.2$ is a numerical constant, and an "effective barrier" F_{eff} has been defined. The latter is a meaningful interpretation since Fig. 7(b) shows that Q is a *constant* preexponential factor, which is essentially identical for $R_g/R=0.06$ and 0.09 ($Q\sim -26.5$) and modestly smaller for the $R_g/R=0.025$ ($Q\sim -30.5$). The very small value of Q is not surprising since it represents an "apparent" prefactor only, not a physical property; the important point is that Q is nearly constant, independent of all system variables. The shapes of all three "master curves" in Fig. 7(b) are virtually identical, and the $R_g/R=0.025$ results can be collapsed (not shown) onto the other two sets of calculations by either a rigid upward shift, or modest change of the fractional exponent in the size asymmetry ratio dependence from 0.75 to 0.68. Equations (20) and (21) are of practical importance since experiments cannot separate contributions from the dynamical prefactor and barrier to the observed relaxation time. Since Kramers theory is only valid for barriers in excess of k_BT, Eq. (21) applies over essentially the entire regime of validity of the calculation.

It is interesting to note that the form of the effective barrier in Eq. (21) is qualitatively identical (similar) to the AO contact value of Eq. (18), or the dilute particle limit of PRISM theory result [5] of $(27/8)(R/R_g)(c_p/c_p^*)$, with regards to the polymer concentration (inverse size asymmetry ratio) dependence. Moreover, in the dilute limit the numerical prefactor of the effective barrier is $c_1 G \sim 2$, again close to the AO result. We do not have a deep understanding of these surprising simplicities since Eq. (21) emerges from the numerical calculations as the combined consequence of the barrier and dynamical prefactor in Eq. (6). In an attempt to gain more insight and explicitly make qualitative contact with the analog of the AO "effective pair potential" between particles, we consider the integral equation version of a renormalized pair attraction strength which includes many body effects: the effective direct correlation function at contact $C_{\text{eff}}(r=D)$. Figure 8 shows that over a wide range of volume frac-

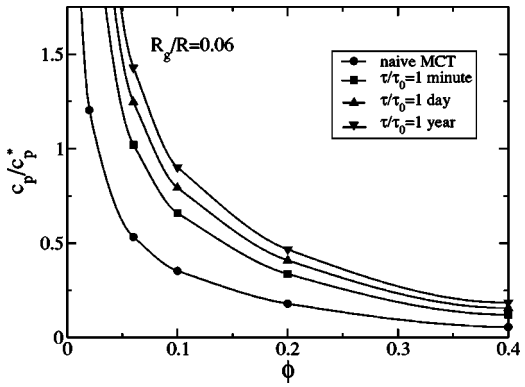

FIG. 9. Kinetic fluid-gel boundary for $R_g/R=0.06$ defined as when the hopping time equals 1 minute (squares), 1 day (triangles), and 1 year (inverse triangles) for an elementary Brownian time of $\tau_0=5.7$ ms. The ideal MCT gel boundary (circles) is shown for comparison.

tions $C_{\mathrm{eff}}(r=D)$ is strongly correlated with the AO-like measure of depletion strength $(R/R_g)(c_p/c_p^*)$. Of course, in contrast to the dilute particle theories $C_{\mathrm{eff}}(r=D)$ increases with volume fraction in a manner that can be fit in many ways including a low order polynomial or the exponential law shown in Fig. 8. A naive interpretation in the AO language might be that $C_{\mathrm{eff}}(r=D)/[(1.5R/R_g)(c_p/c_p^*)]$ quantifies the "number of contact depletion bonds" per particle. Adopting this perspective, the results in Fig. 8 imply the physically reasonable result of 2–5 "bonds" per particle as the volume fraction increases from ~0.1 to 0.4.

B. Kinetic gelation boundaries

Prior work has suggested the naive MCT-PRISM approach can provide a surprisingly good description of the shape, and even the quantitative location, of experimental fluid-gel boundaries [26]. However, if the crisp MCT singularity is destroyed and replaced by a barrier hopping process then, in analogy with a glass transition, a gelation boundary can only be defined kinetically as when the relaxation (hopping) time exceeds a characteristic experimental time scale. The question then arises: how different will such kinetic gel boundaries be compared to their ideal MCT analogs? This issue can be *generically* explored using Eqs. (6), (14), and (15) and (19). to define a kinetic gel boundary analytically as when the hopping time exceeds a prescribed experimental time scale. The kinetic gel boundaries thus defined will depend to some degree on material-specific factors such as colloid size, solvent viscosity, and all the system parameters that determine the effective barrier and dynamic prefactor.

A numerical example relevant to recent experiments is given in Fig. 9 for $R_g/R=0.06$. A value of $\tau_0\sim 0.0057$ s is chosen which corresponds to ~100 nm diameter silica nanoparticles in decalin at room temperature [12,13]. The kinetic gel boundary is defined as when the hopping time equals a selected time scale ranging from one minute to one year. The kinetic gel boundaries necessarily occur at higher reduced polymer concentrations than the naïve MCT predictions, but only by a factor of 2–3 over a wide range of volume fractions. The modest nature of the gel boundary shifts reflects the rapid growth of the barrier with polymer concentration. Moreover, the shape of the kinetic gel boundaries is nearly identical to the results of Eqs. (2) and (3). For example, the kinetic gel boundaries follow the power law form in Eq. (2) with slightly (~10%) larger effective exponents. Hence, naive MCT appears to be a reliable approach for predicting the shape and location of kinetic gel boundaries, and the previously demonstrated good agreement with experiment [26] for this aspect is not fortuitous.

C. Gel collapse

Kilfoil *et al.* [34] have recently studied the effect of aging and gravity-driven gel collapse for a large colloid (silica)–biopolymer (carboxymethylcellulose) suspension. The silica radius is 250 nm, implying a Brownian time of $\tau_0\sim 1$ s. The polymer molecular weight was 60 000, but R_g was not reported; a *very* crude estimate might be ~6 nm which would yield $R/R_g\sim 40$. The time scale τ for the onset of gel collapse was measured as function of polymer concentration for five samples with volume fractions in the range $\phi=0.06-0.2$. The characteristic collapse times fall in the range of 10–700 h. The question is whether our barrier hopping time is relevant to these experiments as an initial event that triggers gravity-driven macroscopic gel collapse.

Experiments find the gel collapse time increases dramatically with increasing polymer concentration and ϕ. For fixed colloid volume fraction, τ depends exponentially on polymer concentration, $\tau\sim\tau_0\exp[b(\phi)c_p]$, in agreement with Eq. (21) and the results in Fig. 7. The effect of volume fraction on the polymer concentration dependence was described by an empirical function $b(\phi)$ which was found to be a linear function of volume fraction for the four samples in the range $\phi=0.1-0.2$. This implies an exponential dependence of the gel collapse time on colloid volume fraction, again in agreement with the results of Fig. 7. For the $\phi=0.06$ sample $b(\phi)$ was roughly the same as for the $\phi=0.1$ sample. This observation is puzzling. For a truly nonergodic gel we do not expect the hopping time should be independent of volume fraction. Whether it reflects new physics is important at very low volume fractions, such as a different cluster structure of the gel, hopping or depletion bond breaking not being the rate limiting step for macroscopic gel collapse, or strong hydrodynamic effects (solvent flow), is unclear.

It seems useful to try to check if the theory can rationalize the order of magnitude of the observed collapse times. For a 20% volume fraction suspension with 0.5% polymer by weight (corresponds roughly to $c_p/c_p^*\sim 0.2$ [45]) the collapse time is ~700 h $\sim 2\times 10^6$ s. From Fig. 7, for this volume fraction, $\tau_0\sim 1$ s, and assuming $R/R_g=40$, we find $\tau/\tau_0\sim 10^2-10^9$ s for $c_p/c_p^*\sim 0.16-0.25$. Since $c_p^*\propto R_g^{-3}$, the latter range of c_p/c_p^* follows from only a ~15% variation of R_g. The hopping time is extremely sensitive to reduced polymer concentration due to the exponential dependence in Eq. (21); it also is predicted to increase strongly with R/R_g. Thus, accurate knowledge of R_g is necessary input to quantitative predictions of the theory via both the R_g/R ratio and c_p^*. Hence, given the absence of accurate experimental knowl-

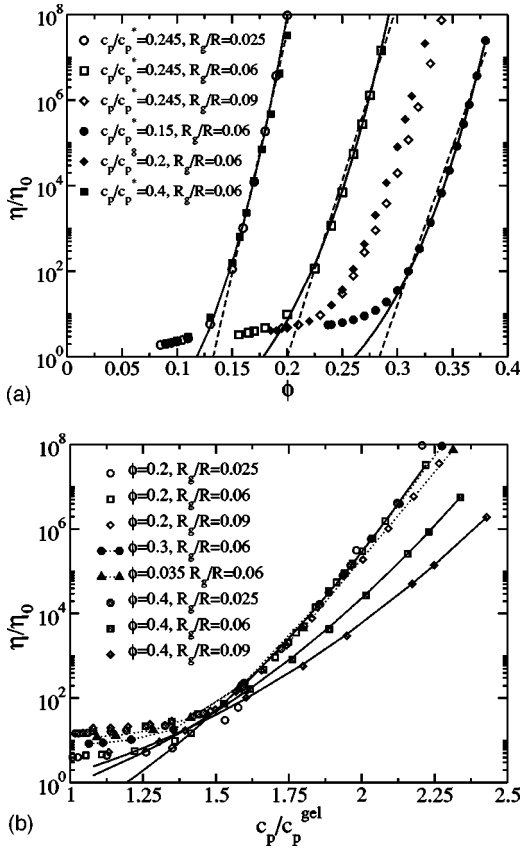

FIG. 10. Relative viscosity as a function of (a) colloid volume fraction and (b) reduced polymer concentration. Solid lines are stretched exponential fits and dashed lines are simple exponential fits. Dotted lines in (b) are only guides to the eye.

edge of R_g and how nonadsorbing on silica this biopolymer is, definitive quantitative conclusions are problematic, but it does seem the absolute magnitude of computed hopping times are plausible. More experiments are needed on well characterized model polymer-colloid suspensions, and the role of polymer-particle size asymmetry ratio needs to be established.

V. SHEAR VISCOSITY

The shear viscosity of polymer-colloid suspensions has been computed using the PRISM and barrier hopping theories plus Eqs. (10)–(12) over the same wide range of polymer concentrations, colloid volume fractions, and size asymmetry ratios studied in Secs. III and IV [46]. Figure 10(a) [Fig. 10(b)] shows a log-linear plot of the viscosity over nearly eight orders of magnitude variation as a function of volume fraction (polymer concentration) for three values of the size asymmetry ratio. In all cases, a relatively weak increase of the viscosity near the MCT gel boundary is followed by a smooth, but rather sharp, crossover to a much stronger dependence.

The numerical results can be described in many ways. A two-exponential regime interpretation of the volume fraction dependences is plausible. Figure 10(a) shows that the highest 5–6 orders of magnitude are rather well fitted as $\sim\exp(\lambda\phi)$; the "activation" prefactor for different polymer concentrations and size asymmetry ratios fall in the range of $\lambda \sim 170-260$. As true for the dimensionless hopping time in the format of Eq. (21), the numerical prefactor is very small. The data in Fig. 10(a) can also be collapsed rather well by empirical horizontal rescaling of the volume fraction (not shown), but the required scaling factor is not simply related to polymer concentration, size asymmetry ratio, nor the ideal MCT gel volume fraction.

Figure 10(a) also demonstrates that an alternative stretched exponential function very accurately describes seven or more orders of magnitude of the high viscosity regime data

$$\frac{\eta}{\eta_0} = C\exp(b\phi^{\Delta}) \tag{22}$$

where $C\sim 0.006-0.06$ and $b\sim 1900\pm 600$. Curiously, we find the best fit effective stretching exponent is remarkably well described by a linear function of the ideal MCT gelation volume fraction: $\Delta = 2.0 + 10.4\phi_{\rm gel}$. Hence, an interesting and potentially testable correlation between the volume fraction dependence of the viscosity and the absolute magnitude of the ideal gelation volume fraction is predicted.

Figure 10(b) shows that the concentration dependence of the viscosity can also be interpreted in a two-regime manner. Moreover, if the polymer concentration is nondimensionalized by its ideal MCT gel value, then a nearly universal master curve is found for $\phi\sim 0.1-0.35$ (not all shown in the figure). The high viscosity regime can again be well fitted over many orders of magnitude by a stretched exponential

$$\frac{\eta}{\eta_0} \propto \exp\left[d\left(\frac{c_p}{c_p^{\rm gel}}\right)^{\mu}\right] \tag{23}$$

where $\mu\sim 2.3$ and is largely insensitive to volume fraction or size asymmetry ratio, and $d\sim 3.6$ over a range of volume fractions. However, systematic deviations from this nearly universal behavior emerge at the highest volume fraction of 40% in a manner that depends strongly on the size asymmetry ratio. This might reflect interference between the consequences of depletion attraction and repulsive force caging effects which become increasingly important as the glassy volume fraction regime is approached [29].

All the numerical viscosity results in the three-dimensional parameter space of volume fraction, polymer concentration and size asymmetry ratio have been plotted in multiple ways in an attempt to discover an underlying simplicity. Given the dominance of the hopping friction in Eqs. (10)–(12) for the viscosity, and the central role played by the barrier in determining the hopping time, a strong exponential correlation between viscosity and barrier seems likely. This is explicitly demonstrated in Fig. 11. A near collapse of all the viscosity results is found beyond the threshold regime [low barrier $F_B < (3-5)k_BT$]. The corresponding master function is

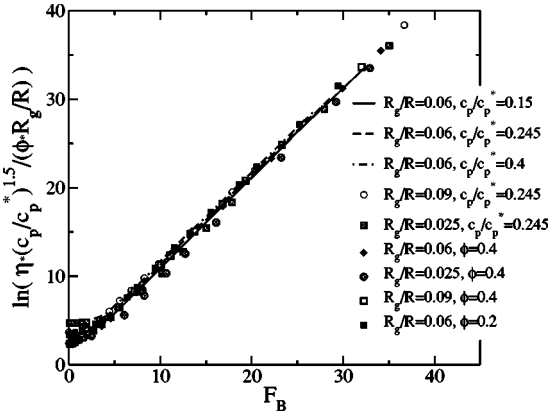

FIG. 11. Natural log-linear plot of the viscosity multiplied by the indicated scaling prefactor as a function of barrier height for a wide range of size asymmetry ratios, volume fractions, and reduced polymer concentrations. For a fixed volume fraction (polymer concentration) different points correspond to different polymer concentrations (volume fractions).

$$\frac{\eta}{\eta_0} \propto \phi \frac{R_g}{R} \left(\frac{c_p}{c_p^*} \right)^{-1.5} \exp(F_B). \tag{24}$$

The simple form of the prefactor is not easy to understand since many factors enter in its determination including the well and barrier curvatures, the short time friction constant, and the structure factor and its derivative which quantify the "vertex" and Debye-Waller factor in the Green-Kubo expression Eq. (10). Apparently, the rather significant dependence of each of these different factors on ϕ, size asymmetry ratio, and polymer concentration largely cancels out resulting in the weak prefactor dependences in Eq. (24). Use of the simpler Maxwell model expression for the viscosity in Eq. (8) yields qualitatively identical behavior as found for the Green-Kubo based analysis.

By combining Eqs. (14)–(16) with Eq. (24) an *analytic expression* for the dependence of the viscosity on the three material control parameters is obtained which should be useful for interpreting experiments. Buscall *et al.* [35] have measured the shear viscosity of model polymer-colloid depletion systems over many orders of magnitude and find an exponential dependence on polymer concentration which is qualitatively consistent with our theoretical results. Although we have not computed the self-diffusion constant D_s, this is easily done using the results of this paper and prior work [32]. Previous studies of glassy hard sphere suspensions with the present Green-Kubo based approach found a Stokes-Einstein-like behavior holds [32], so $D_s \sim \eta^{-1}$ is also expected for the depletion systems. Of course, "dynamic heterogeneity" [47], associated with a mesoscale domain picture and/or fluctuations in the barrier hopping time beyond the mean first passage time Kramers approach, has not been explicitly taken into account. The barrier hopping theory has been generalized to include both the former aspect (and applied to hard sphere suspensions) [48], and the latter aspect based on numerical solution of the full stochastic theory of Eq. (4) [49].

VI. DISCUSSION AND SUMMARY

The microscopic naive MCT-PRISM theory of depletion-driven particle gelation has been extended to treat the emergence of barriers and activated transport. The barrier makes the dominant contribution to the hopping or α relaxation time and shear viscosity, and is a rich function of the depletion attraction strength via the polymer concentration, polymer-particle size asymmetry ratio, and particle volume fraction. The dependence of the barrier on these control parameters can be accurately collapsed onto a single scaling variable, and the resultant master function is well described by a simple power law. Given the ability to treat activated events and long time transport processes, a theory for kinetic gel boundaries has been formulated and applied to interpret the phenomenon of delayed gel flow and collapse. The form of the kinetic gel lines is qualitatively the same as obtained from prior naive MCT-PRISM studies [26]. Hence, the previously documented good agreement of naive MCT-PRISM predictions for fluid-gel boundaries and the elastic shear modulus with experiments is not destroyed by the introduction of barriers and hopping transport. The "onset" of slow dynamics, and the elastic modulus (or the localization length) of the transient nonergodic ("caged") state, are expected to be well described by ideal MCT.

As true of all prior MCT type theories, there are potential limitations of our approach. These include the role of global gel connectivity, percolation, fractal or dense aggregate formation, gravity-induced sedimentation, hydrodynamics, and/or metastable phase separation boundaries. In any specific real material these poorly understood effects may or may not be important. We believe these complications are most relevant for relatively low volume fraction suspensions which have not been buoyancy matched.

A dynamical theory for quantities such as the colloid mean square displacement, distribution of hopping times, non-Gaussian parameter, and incoherent dynamic structure factor has not been worked out. However, this is not a fundamental limitation and can be addressed by employing Brownian dynamics simulation to solve the nonlinear stochastic Langevin equation of the theory; work in this direction is in progress [49]. Finally, the methods and ideas developed in this paper can be generalized to treat nonlinear viscoelasticity of depletion gels and phenomena such as yielding, strain softening, and shear thinning. Such a generalization was recently carried out for glassy hard sphere suspensions [50], and its application to depletion gels will be reported elsewhere [51].

ACKNOWLEDGMENTS

This work was supported by the Nanoscale Science and Engineering Initiative of the National Science Foundation under NSF Award No. DMR-0117792, and the U.S. Department of Energy, Division of Materials Sciences under Award No. DEFG02-91ER45439 through the UIUC Frederick Seitz Materials Research Laboratory. Helpful discussions and correspondence with Professor Maria Kilfoil concerning her experiments are gratefully acknowledged.

[1] S. Asakura and F. Oosawa, J. Chem. Phys. **22**, 1255 (1954).
[2] S. Asakura and F. Oosawa, J. Polym. Sci. **33**, 183 (1958).
[3] P. G. Bolhuis, A. A. Louis, and J.-P. Hansen, Phys. Rev. Lett. **89**, 128302 (2002).
[4] Y. L. Chen, K. S. Schweizer, and M. Fuchs, J. Chem. Phys. **118**, 3880 (2003).
[5] M. Fuchs and K. S. Schweizer, Europhys. Lett. **51**, 621 (2000); J. Phys.: Condens. Matter **514**, R239 (2002); Phys. Rev. E **64**, 021514 (2001).
[6] E. Eisenriegler, J. Chem. Phys. **113**, 5091 (2000).
[7] H. N. W. Lekkerkerker, W. C. K. Poon, P. N. Pusey, A. Stroobants, and P. B. Warren, Europhys. Lett. **20**, 559 (1992).
[8] W. C. K. Poon, J. Phys.: Condens. Matter **14**, R859 (2002).
[9] V. Prasad, V. Trappe, A. D. Dinsmore, P. N. Segre, L. Cipelletti, and D. A. Weitz, Faraday Discuss. **123**, 1 (2003).
[10] S. Ramakrishnan, M. Fuchs, K. S. Schweizer, and C. F. Zukoski, J. Chem. Phys. **116**, 2201 (2002).
[11] R. P. Sear, Phys. Rev. Lett. **86**, 4696 (2001).
[12] S. A. Shah, Y. L. Chen, K. S. Schweizer, and C. F. Zukoski, J. Chem. Phys. **118**, 3350 (2003).
[13] S. A. Shah, Y. L. Chen, S. Ramakrishnan, K. S. Schweizer, and C. F. Zukoski, J. Phys.: Condens. Matter **15**, 4751 (2003).
[14] G. A. Vliegenthart, A. v. Blaaderen, and H. N. W. Lekkerkerker, Faraday Discuss. **112**, 173 (1999).
[15] S. M. Ilett, A. Orrock, W. C. K. Poon, and P. N. Pusey, Phys. Rev. E **51**, 1344 (1995).
[16] W. C. K. Poon, A. D. Pirie, M. D. Haw, and P. N. Pusey, Physica A **235**, 110 (1997).
[17] S. A. Shah, S. Ramakrishnan, Y. L. Chen, K. S. Schweizer, and C. F. Zukoski, Langmuir **19**, 5128 (2003).
[18] S. A. Shah, Y. L. Chen, K. S. Schweizer, and C. F. Zukoski, J. Chem. Phys. **119**, 8747 (2003).
[19] L. Starrs, W. C. K. Poon, D. J. Hibberd, and M. M. Robbins, J. Phys.: Condens. Matter **14**, 2485 (2002).
[20] W. C. K. Poon, A. D. Pirie, and P. N. Pusey, Faraday Discuss. **101**, 65 (1995).
[21] J. Bergenholtz, W. C. K. Poon, and M. Fuchs, Langmuir **19**, 4493 (2003).
[22] J. Bergenholtz, M. Fuchs, and T. Voigtmann, J. Phys.: Condens. Matter **12**, 6575 (2000).
[23] J. Bergenholtz and M. Fuchs, J. Phys.: Condens. Matter **11**, 10171 (1999).
[24] J. Bergenholtz and M. Fuchs, Phys. Rev. E **59**, 5706 (1999).
[25] L. Fabbian, W. Götze, F. Sciortino, P. Tartaglia, and F. Thiery, Phys. Rev. E **59**, R1347 (1999).
[26] Y.-L. Chen and K. S. Schweizer, J. Chem. Phys. **120**, 7212 (2004).
[27] K. Dawson, G. Foffi, M. Fuchs, W. Götze, F. Sciortino, M. Sperl, P. Tartaglia, T. Voigtmann, and E. Zaccarelli, Phys. Rev. E **63**, 011401 (2000); E. Zaccarelli, G. Foffi, K. A. Dawson, F. Sciortino, and P. Tartaglia, *ibid.* **63**, 031501 (2001).
[28] K. N. Pham, A. M. Puertas, J. Bergenholtz, S. U. Egelhaaf, A. Moussaid, P. N. Pusey, A. B. Schofield, M. E. Cates, M. Fuchs, and W. C. K. Poon, Science **296**, 104 (2002).
[29] W. Götze, *Liquids, Freezing and the Glass Transition* (North-Holland, Amsterdam, 1991); J. Phys.: Condens. Matter **11**, A1 (1999).
[30] S. Ramakrishnan, Y.-L. Chen, K. S. Schweizer, and C. F. Zukoski, Phys. Rev. E **70**, 040401(R) (2004).
[31] T. R. Kirkpatrick and P. G. Wolynes, Phys. Rev. A **35**, 3072 (1987).
[32] K. S. Schweizer and E. J. Saltzman, J. Chem. Phys. **119**, 1181 (2003); E. J. Saltzman and K. S. Schweizer, *ibid.* **119**, 1197 (2003).
[33] E. Zacarelli, G. Foffi, F. Scirotino, and P. Tattaglia, Phys. Rev. Lett. **91**, 108301 (2003).
[34] M. Kilfoil, E. E. Pashkovski, J. A. Masters, and D. A. Weitz, Philos. Trans. R. Soc. London, Ser. A **361**, 753 (2003).
[35] R. Buscall, J. I. McGowan, and A. J. Morton-Jones, J. Rheol. **37**, 621 (1993).
[36] P. G. de Gennes, *Scaling Concepts in Polymer Physics* (Cornell University Press, Ithaca, NY, 1979).
[37] J. M. Mendez and R. Klein, Phys. Rev. E **61**, 4095 (2000).
[38] D. Oxtoby, *Liquids, Freezing and the Glass Transition* (North-Holland, Amsterdam, 1991); A. J. Archer and M. Rausher, J. Phys. A **37**, 9325 (2004), and references therein.
[39] N. Goldenfeld, *Lectures on Phase Transitions and the Renormalization Group* (Addison-Wesley Company, New York, 1992).
[40] E. G. D. Cohen, R. Vergberg, and I. M. deSchepper, Physica A **251**, 251 (1998).
[41] J. P. Hansen and I. R. McDonald, *Theory of Simple Liquids* (Academic, London, 1986).
[42] K. S. Schweizer (unpublished).
[43] H. A. Kramers, Physica (Amsterdam) **7**, 284 (1940).
[44] R. G. Larson, *The Structure and Rheology of Complex Fluids* (Oxford University Press, New York, 1999).
[45] M. Kilfoil (private communication).
[46] The viscosity calculations were performed using the hard sphere contact value in the prefactor of the hopping time. The consequences of this simplification are extremely small given the dominance of the barrier in the viscosity calculation.
[47] M. D. Ediger, Annu. Rev. Phys. Chem. **51**, 99 (2000).
[48] K. S. Schweizer and E. J. Saltzman, J. Phys. Chem. B **108**, 19729 (2004).
[49] E. J. Saltzman, V. Kobelev, and K. S. Schweizer (unpublished).
[50] V. Kobelev and K. S. Schweizer, Phys. Rev. E **71**, 021401 (2005).
[51] V. Kobelev and K. S. Schweizer (unpublished).